 CMC, vol.44, no.2, pp.123-140, 2014

Sensitivity of Dynamic Response of a Simply Supported Functionally Graded Magneto-electro-elastic Plate to its Elastic Parameters

G. Q. Xie[1,2] and M. X. Chi[1]

Abstract: Dynamic response sensitivity of a simply supported functionally graded magneto- electro-elastic plates have been studied by combining analytical method with finite element method. The functionally graded material parameters are assumed to obey exponential law in the thickness direction. A series solution of double trigonometric function agreed with the simply supported boundary condition is adopted in the plane of the plate and finite element method is used across the thickness of the plate. The finite element model is established based on energy variational principle. The coupled electromagnetic dynamic characteristics of a simply supported functionally graded magneto- electro-elastic plate are decided by its dynamics differential equation into which displacement components, electric potential and magnetic potential as nodal degree of freedom are incorporated. Dynamic response sensitivity is defined as a partial differential of dynamic response with respect to material parameter. Sensitivity of dynamic response of a simply supported functionally graded magneto-electro-elastic plate to its elastic parameters has been studied. The influence of the different exponential factor on dynamic response sensitivity has also been investigated.

Keywords: Dynamic response sensitivity, simply supported functionally graded magneto-electro- elastic plate, elastic parameters, finite element method, double trigonometric function.

1 Introduction

Many scholars have increasingly focused on the properties of magneto-electro-elastic structures employed as these smart or intelligent materials have ability of converting energy from one form to the other (among magnetic, electric and me-

[1] Civil Engineering College, Hunan University of Science and Technology, Xiangtan, PR China, 411201.
[2] Corresponding author. E-mail: xiaoyuanyixiong@163.com

chanical energy) [Nan (1994); Harshe et al. (1993)]. Applied in ultrasonic imaging devices, sensors, actuators, transducers and many other emerging components, it is a strong necessity for these smart or intelligent materials and structure to study dynamic and static characteristics of theses by theories or techniques. Static and dynamic behavior of plates as well as infinite cylinder has been studied in the literature. Pan (2001) obtained an exact closed-form solution for the simply supported and multilayered plate composed of anisotropic piezoelectric and piezomagnetic materials under a static mechanical load. Pan and Heyliger (2002) solved the corresponding dynamic problem. Static behavior of a functionally graded magneto-electro-elastic hollow sphere subjected to hydrothermal loading in the spherically symmetric state was studied by M. Saadatfar and M. Aghaie-Khafri (2014). The dynamic response of a rotating radically polarized functionally graded piezoelectric hollow cylinder was investigated by A. H. Akbarzadeh and Z. T. Chen (2012). Coupling effect of electric and magnetic fields was found in piezoelectric and piezomagnetic composites. Jianguo Wang and Xuefeng Li (2008) derived analytical solutions for the magneto-electric effect of multilayered magneto-electro-elastic media by using the transfer matrix method. M R Sedighi and M. Shakeri (2009) obtained a three-dimensional elasticity solution of functionally graded piezoelectric cylindrical panels. Bishay, Sladek, Sladek and Atluri (2012) used hybrid/mixed finite elements and node-wise material properties to analyze functionally graded magneto-electro-elastic composites Buchanan (2004) used finite element method to study the behavior of layered versus multiphase magneto-electro-elastic infinite long plate composites Wang et al. (2003) had carried out analysis of multilayered magnetoelectro-elastic plates for mechanical and electrical loading by the state vector approach. Free vibration of a magneto-electro-elastic plate resting on a Pasternak foundation was investigated by Yansong Li and Jingjun Zhang (2014) based on Mindlin theory Rajesh K. Bhangale and N. Ganesan (2006) derived semi-analytical finite element method to static analysis of simply supported functionally graded and layered magneto-electro-elastic plates In the present study, a series solution in conjunction with finite element approach is extended to dynamic response sensitivity analysis of a functionally graded magneto-electro-elastic plates The studies on dynamic sensitivity analysis of the functionally graded magnetoelectro-elastic structure to material parameters is less in the literature, Dynamic response sensitivity analysis is essential to optimization design and inverse technique of smart material.

2 Basic equations

The coupled physic equations for anisotropic and linear magneto-electro-elastic solids are given by:

$$\left.\begin{array}{l}\boldsymbol{\sigma}=\mathbf{C}\boldsymbol{\varepsilon}-\mathbf{e}^T\mathbf{E}-\mathbf{q}^T\mathbf{H}\\ \mathbf{D}=\mathbf{e}\boldsymbol{\varepsilon}+\mathbf{g}\mathbf{E}+\boldsymbol{\alpha}^T\mathbf{H}\\ \mathbf{B}=\mathbf{q}\boldsymbol{\varepsilon}+\alpha\mathbf{E}+\boldsymbol{\mu}\boldsymbol{H}\end{array}\right\} \tag{1}$$

Where $\boldsymbol{\sigma}=\left[\begin{array}{cccccc}\sigma_x & \sigma_y & \sigma_z & \sigma_{yz} & \sigma_{zx} & \sigma_{xy}\end{array}\right]^T$ denotes stress vector, $\varepsilon=\left[\begin{array}{cccccc}\varepsilon_x & \varepsilon_y & \varepsilon_z & \varepsilon_{yz} & \varepsilon_{zx} & \varepsilon_{xy}\end{array}\right]^T$ denotes strain vector, $\mathbf{D}$ is the electric displacement vector and $\boldsymbol{B}$ is the magnetic induction vector $\boldsymbol{C}$, $\boldsymbol{g}$ and $\boldsymbol{\mu}$ are the elastic, dielectric and magnetic permeability coefficient matrices $\boldsymbol{q}$, $\boldsymbol{e}$ and $\boldsymbol{\alpha}$ are piezoelectric, piezo-magnetic and magnetoelectric material coefficient matrices.

The strain–displacement relations are

$$\boldsymbol{\varepsilon}=\mathbf{L}_d\mathbf{U} \tag{2}$$

Where

$$\mathbf{U}^T=\left\{\begin{array}{ccc}u & v & w\end{array}\right\} \tag{3}$$

The operator $\mathbf{L}_d$ is

$$\mathbf{L}_d=\left[\begin{array}{cccccc}\frac{\partial}{\partial x} & 0 & 0 & 0 & \frac{\partial}{\partial z} & \frac{\partial}{\partial y}\\ 0 & \frac{\partial}{\partial y} & 0 & \frac{\partial}{\partial z} & 0 & \frac{\partial}{\partial x}\\ 0 & 0 & \frac{\partial}{\partial z} & \frac{\partial}{\partial y} & \frac{\partial}{\partial x} & 0\end{array}\right]^T \tag{4}$$

In Eq. (3), u, v, w are elastic displacement component in coordinate directions x, y and z, respectively

The electric field vector $\boldsymbol{E}$ is related to the electric potential φ as follows:

$$\mathbf{E}=-\mathbf{L}_\varphi\varphi \tag{5}$$

The relations between magnetic field and magnetic potential are given by:

$$\mathbf{H}=-\mathbf{L}_\varphi\psi \tag{6}$$

In Eq. (5) and Eq. (6), $\mathbf{L}_\varphi$ is an operator as shown below:

$$\mathbf{L}_\varphi=\left(\frac{\partial}{\partial x},\frac{\partial}{\partial y},\frac{\partial}{\partial z}\right)^T \tag{7}$$

3 Dynamics differential equation

The functionally graded material parameters are assumed to obey exponential law in the thickness direction. The plate is divided into 3 nodal surfaces namely upper, middle and lower nodal surfaces in the thickness z direction. The following shape functions are adopted

$$\left.\begin{array}{l}\mathbf{N}_d(z)=[N_1\mathbf{I},N_2\mathbf{I},N_3\mathbf{I}]\\ \mathbf{N}_\varphi(z)=[N_1,N_2,N_3]\end{array}\right\}\tag{8}$$

Where $N_1=\left(1-3\bar{z}+2\bar{z}^2\right)$, $N_2=4\left(\bar{z}-\bar{z}^2\right)$, $N_3=\left(2\bar{z}^2-\bar{z}\right)$, $\bar{z}=z_i-z_{i-1}/h$, I is a 3×3 identity matrix, h is the thickness of the plate.

The displacement $\boldsymbol{U}$ and the electrostatic potential φ and the static magnetic potential ψ are approximated by the shape functions and the degrees of freedom of 3 nodal surfaces.

$$\begin{array}{l}\mathbf{U}(x,y,z,t)=\mathbf{N}_d(z)\,\mathbf{d}(x,y,t)\\ \varphi(x,y,z,t)=\mathbf{N}_\varphi(z)\,\boldsymbol{\varphi}(x,y,t)\\ \psi(x,y,z,t)=\mathbf{N}_\varphi(z)\,\boldsymbol{\psi}(x,y,t)\end{array}\tag{9}$$

Where

$$\left\{\begin{array}{l}\mathbf{d}^T=\left\{\mathbf{d}_l^T\quad\mathbf{d}_m^T\quad\mathbf{d}_u^T\right\},\mathbf{d}_i^T=\left\{\begin{array}{ccc}u_i & v_i & w_i\end{array}\right\}\\ \boldsymbol{\varphi}^T=\left\{\begin{array}{ccc}\varphi_l & \varphi_m & \varphi_u\end{array}\right\}\\ \boldsymbol{\psi}^T=\left\{\begin{array}{ccc}\psi_l & \psi_m & \psi_u\end{array}\right\}\end{array}\right.\tag{10}$$

Where $i=l,m,u$, l denotes lower nodal surface, m middle nodal surface and u upper nodal surface.

In the present work a set of finite series solution agreed with the boundary conditions for the simply supported rectangular plates $(a\times b)$ has been adopted. The generalized displacement functions are as follows:

$$\left\{\begin{array}{l}u(x,y,t)=\sum\limits_{m=1}^{M}\sum\limits_{n=1}^{N}U_{mn}(t)\cos\frac{m\pi x}{a}\sin\frac{n\pi y}{b}\\ v(x,y,t)=\sum\limits_{m=1}^{M}\sum\limits_{n=1}^{N}V_{mn}(t)\sin\frac{m\pi x}{a}\cos\frac{n\pi y}{b}\\ w(x,y,t)=\sum\limits_{m=1}^{M}\sum\limits_{n=1}^{N}W_{mn}(t)\sin\frac{m\pi x}{a}\sin\frac{n\pi y}{b}\\ \varphi(x,y,t)=\sum\limits_{m=1}^{M}\sum\limits_{n=1}^{N}\varphi_{mn}(t)\sin\frac{m\pi x}{a}\sin\frac{n\pi y}{b}\\ \psi(x,y,t)=\sum\limits_{m=1}^{M}\sum\limits_{n=1}^{N}\Psi_{mn}(t)\sin\frac{m\pi x}{a}\sin\frac{n\pi y}{b}\end{array}\right.\tag{11}$$

Where n and m are two positive integers, N and M are the term number of the series to be accounted for the general excitation.

Coupled equations of a finite layer element are given by:

$$\mathbf{M}_e\ddot{\mathbf{V}}_e+\mathbf{K}_e\mathbf{V}_e=\mathbf{T}_e \tag{12}$$

Where

$$\mathbf{V}_e^T=\left\{\boldsymbol{\Theta}^T,\boldsymbol{\varphi}^T,\boldsymbol{\Psi}^T\right\} \tag{13}$$

$$\mathbf{T}_e^T=\int_0^a\int_0^b\left\{\mathbf{F}^T,\mathbf{D}_z^T,\mathbf{B}_z^T\right\}\mathrm{d}x\mathrm{d}y \tag{14}$$

$$\mathbf{M}_e=\begin{bmatrix}\mathbf{M}_s & \mathbf{0} & \mathbf{0}\\ \mathbf{0} & \mathbf{0} & \mathbf{0}\\ \mathbf{0} & \mathbf{0} & \mathbf{0}\end{bmatrix} \tag{15}$$

$$\mathbf{K}_e=\begin{bmatrix}\mathbf{K}_{dd} & \mathbf{K}_{d\varphi} & \mathbf{K}_{d\psi}\\ \mathbf{K}_{d\varphi}^T & -\mathbf{K}_{\varphi\varphi} & -\mathbf{K}_{\varphi\psi}\\ \mathbf{K}_{d\psi}^T & -\mathbf{K}_{\varphi\psi}^T & -\mathbf{K}_{\psi\psi}\end{bmatrix} \tag{16}$$

In Eq. (13)

$$\left\{\begin{array}{l}\boldsymbol{\Theta}^T=\left\{\begin{array}{ccc}\boldsymbol{\Theta}^l & \boldsymbol{\Theta}^m & \boldsymbol{\Theta}^u\end{array}\right\},\boldsymbol{\Theta}^i=\left\{\begin{array}{ccc}U_{mn}^i & V_{mn}^i & W_{mn}^i\end{array}\right\}\\ \varphi^T=\left\{\begin{array}{ccc}\varphi_{mn}^l & \varphi_{mn}^m & \varphi_{mn}^u\end{array}\right\}\\ \boldsymbol{\Psi}^T=\left\{\begin{array}{ccc}\Psi_{mn}^l & \Psi_{mn}^m & \Psi_{mn}^u\end{array}\right\}\end{array}\right. \tag{17}$$

In Eq. (14)

$$\left\{\begin{array}{l}\mathbf{F}^T=\left\{\begin{array}{ccc}\mathbf{F}^l & \mathbf{F}^m & \mathbf{F}^u\end{array}\right\},\mathbf{F}^i=\left\{\begin{array}{ccc}F_x & F_y & F_z\end{array}\right\}^i\\ \mathbf{D}_z^T=\left\{\begin{array}{ccc}(D_Z)^l & (D_Z)^m & (D_Z)^u\end{array}\right\}\\ \mathbf{B}_z^T=\left\{\begin{array}{ccc}(B_Z)^l & (B_Z)^m & (B_Z)^u\end{array}\right\}\end{array}\right. \tag{18}$$

Where $\boldsymbol{F}$ is the external traction vector applied on the nodal surface.

In Eq. (15)

$$\mathbf{M}_s=c\int_0^h\rho\mathbf{N}^T(z)\mathbf{N}(z)\mathrm{d}z \tag{19}$$

In Eq. (16)

$$\left.\begin{array}{ll}\mathbf{K}_{dd}=c\int_0^{h_n}\tilde{\mathbf{B}}_d^T\mathbf{C}\tilde{\mathbf{B}}_d\mathrm{d}z, & \mathbf{K}_{d\varphi}=c\int_0^{h_n}\tilde{\mathbf{B}}_d^T\mathbf{e}^T\tilde{\mathbf{B}}_\varphi\mathrm{d}z\\ \mathbf{K}_{d\psi}=c\int_0^{h_n}\tilde{\mathbf{B}}_d^T\mathbf{q}^T\tilde{\mathbf{B}}_\psi\mathrm{d}z, & \mathbf{K}_{\varphi\varphi}=c\int_0^{h_n}\tilde{\mathbf{B}}_\varphi^T\mathbf{g}\tilde{\mathbf{B}}_\varphi\mathrm{d}z\\ \mathbf{K}_{\varphi\psi}=c\int_0^{h_n}\tilde{\mathbf{B}}_d^T\alpha^T\tilde{\mathbf{B}}_\psi\mathrm{d}z, & \mathbf{K}_{\psi\psi}=c\int_0^{h_n}\tilde{\mathbf{B}}_\psi^T\mu\tilde{\mathbf{B}}_\psi\mathrm{d}z\end{array}\right\} \tag{20}$$

Where $c = ab/4$

$$\tilde{\mathbf{B}}_d = \begin{bmatrix} \mathbf{B}_1 & \mathbf{B}_2 & \mathbf{B}_3 \end{bmatrix},\ \tilde{\mathbf{B}}_\varphi = \begin{bmatrix} \mathbf{B}_{\varphi 1} & \mathbf{B}_{\varphi 2} & \mathbf{B}_{\varphi 3} \end{bmatrix},\ \tilde{\mathbf{B}}_\psi = \begin{bmatrix} \mathbf{B}_{\varphi_1} & \mathbf{B}_{\varphi 2} & \mathbf{B}_{\varphi 3} \end{bmatrix} \tag{21}$$

Where

$$\mathbf{B}_1^T = \begin{bmatrix} -\frac{m\pi}{a}N_1 & 0 & 0 & 0 & \frac{\partial N_1}{\partial z} & \frac{n\pi}{b}N_1 \\ 0 & -\frac{n\pi}{b}N_1 & 0 & \frac{\partial N_1}{\partial z} & 0 & \frac{m\pi}{a}N_1 \\ 0 & 0 & \frac{\partial N_1}{\partial z} & \frac{n\pi}{b}N_1 & \frac{m\pi}{a}N_1 & 0 \end{bmatrix} \tag{22}$$

$$\mathbf{B}_2^T = \begin{bmatrix} -\frac{m\pi}{a}N_2 & 0 & 0 & 0 & \frac{\partial N_2}{\partial z} & \frac{n\pi}{b}N_2 \\ 0 & -\frac{n\pi}{b}N_2 & 0 & \frac{\partial N_2}{\partial z} & 0 & \frac{m\pi}{a}N_2 \\ 0 & 0 & \frac{\partial N_2}{\partial z} & \frac{n\pi}{b}N_2 & \frac{m\pi}{a}N_2 & 0 \end{bmatrix} \tag{23}$$

$$\mathbf{B}_3^T = \begin{bmatrix} -\frac{m\pi}{a}N_3 & 0 & 0 & 0 & \frac{\partial N_3}{\partial z} & \frac{n\pi}{b}N_3 \\ 0 & -\frac{n\pi}{b}N_3 & 0 & \frac{\partial N_3}{\partial z} & 0 & \frac{m\pi}{a}N_3 \\ 0 & 0 & \frac{\partial N_3}{\partial z} & \frac{n\pi}{b}N_3 & \frac{m\pi}{a}N_3 & 0 \end{bmatrix} \tag{24}$$

$$\mathbf{B}_{\varphi 1} = \begin{bmatrix} \frac{m\pi}{a}N_1 & \frac{n\pi}{b}N_1 & \frac{\partial N_1}{\partial z} \end{bmatrix}^T \tag{25}$$

$$\mathbf{B}_{\varphi 2} = \begin{bmatrix} \frac{m\pi}{a}N_2 & \frac{n\pi}{b}N_2 & \frac{\partial N_2}{\partial z} \end{bmatrix}^T \tag{26}$$

$$\mathbf{B}_{\varphi 3} = \begin{bmatrix} \frac{m\pi}{a}N_3 & \frac{n\pi}{b}N_3 & \frac{\partial N_3}{\partial z} \end{bmatrix}^T \tag{27}$$

Assembling matrices of all the elements, we obtain the entire dynamic differential equation of the functionally graded magneto-electro-elastic plate:

$$\mathbf{M}_T\ddot{\mathbf{V}}_T + \mathbf{K}_T\mathbf{V}_T = \mathbf{T}_T \tag{28}$$

In the present work we only consider sensitivity of dynamic response to material elastic parameters, and take no account of sensitivity of dynamic response to material density mass and dimension sizes.

If a harmonic mechanical traction vector $\mathbf{F}_t = \{A\}_t \sin(\omega t)$ is applied on the top surface of the plate, and in Eq. (11) $m = n$=1 is adopted, the solution corresponding to Eq. (28) has the form:

$$\begin{cases} u(x,y,z,t) = U_{11}\sin(\omega t)\cos\frac{m\pi x}{a}\sin\frac{n\pi y}{b} \\ v(x,y,z,t) = V_{11}\sin(\omega t)\sin\frac{m\pi x}{a}\cos\frac{n\pi y}{b} \\ w(x,y,z,t) = W_{11}\sin(\omega t)\sin\frac{m\pi x}{a}\sin\frac{n\pi y}{b} \\ \varphi(x,y,z,t) = \varphi_{11}\sin(\omega t)\sin\frac{m\pi x}{a}\sin\frac{n\pi y}{b} \\ \psi(x,y,z,t) = \Psi_{11}\sin(\omega t)\sin\frac{m\pi x}{a}\sin\frac{n\pi y}{b} \end{cases} \tag{29}$$

Substituting Eq. (29) into Eq. (28), we have

$$
\begin{aligned}
&-\omega^2 [M_s]_t \{\Re\}_t + [K_{dd}]_t \{\Re\}_t + \left[K_{d\varphi}\right]_t \{\varphi\}_t + \left[K_{d\psi}\right]_t \{\Psi\}_t = \{A\}_t \\
&\left[K_{d\varphi}\right]_t^T \{\Re\}_t - \left[K_{\varphi\varphi}\right]_t \{\varphi\}_t - \left[K_{\varphi\psi}\right]_t \{\Psi\}_t = \{D_z\}_t \\
&\left[K_{d\psi}\right]_t^T \{\Re\}_t - \left[K_{\varphi\psi}\right]_t^T \{\varphi\}_t - \left[K_{\psi\psi}\right]_t \{\Psi\}_t = \{B_z\}_t
\end{aligned}
\tag{30}
$$

Where

$$
\{\Re\}_t^T = [U_{11}, V_{11}, W_{11}]_t, \{\varphi\}_t^T = [\varphi_{11}]_t, \{\Psi\}_t^T = [\Psi_{11}]_t \tag{31}
$$

If material elastic parameters are taken as the design variables 'θ', applying a partial differential on Eq. (30) with respect toθ, we have

$$
\begin{aligned}
&-\omega^2 [M_s]_t \frac{\partial \{\Re\}_t}{\partial \theta} + [K_{dd}]_t \frac{\partial \{\Re\}_t}{\partial \theta} + \frac{\partial [K_{dd}]_t}{\partial \theta} \{\Re\}_t \\
&+ \left[K_{d\varphi}\right]_t \frac{\partial \{\varphi\}_t}{\partial \theta} + \left[K_{d\psi}\right]_t \frac{\partial \{\Psi\}_t}{\partial \theta} = \{0\} \\
&\left[K_{d\varphi}\right]_t^T \frac{\partial \{\Re\}_t}{\partial \theta} - \left[K_{\varphi\varphi}\right]_t \frac{\partial \{\varphi\}_t}{\partial \theta} - \left[K_{\varphi\psi}\right]_t \frac{\partial \{\Psi\}_t}{\partial \theta} = \{0\} \\
&\left[K_{d\psi}\right]_t^T \frac{\partial \{\Re\}_t}{\partial \theta} - \left[K_{\varphi\psi}\right]_t^T \frac{\partial \{\varphi\}_t}{\partial \theta} - \left[K_{\psi\psi}\right]_t \frac{\partial \{\Psi\}_t}{\partial \theta} = \{0\}
\end{aligned}
\tag{32}
$$

4 Numerical example

For all the subsequent numerical examples, the functionally graded magneto-electro-elastic plate are taken with the material parameters are given in **Appendix A** Consider a FGM magneto- electro-elastic plate having horizontal dimensions a =0.5m and b=0.5m and thickness h = 0.04m, The mechanic model of the FGM magneto-electro-elastic plate is shown in Fig.1.

The following dimensional parameters are adopted:

$$\bar{x} = x/h,\ \bar{z} = z/h,\ \bar{u} = u/u_0,\ \bar{v} = v/u_0,\ \bar{w} = w/u_0$$

$$u_0 = hq_0/c_{66},\ \bar{\varphi} = \varphi/\varphi_0,\ \varphi_0 = e_s hq_0/(g_s c_{66}),\ \bar{\psi} = \psi/\psi_0,\ \psi_0 = q_s hq_0/(\mu_s c_{66})$$

Where c_{66} = 1GPa. $e_s = 1\mathrm{C/m^2} g_s = 10^{-10}\mathrm{As/Vm}$, $q_s = 1\mathrm{Vs/m^2}$, $\mu_s = 10^{-6}\mathrm{Vs/Am^2}$. For the mechanical loads, $q_0 = 1\mathrm{N/m^2}$ and for the electrode excitation, $q_0 = e_s p_0/h$, p_0 is a constant expressing the value of the electrostatic potential, and for the magnetic pole excitation, $q_0 = e_s p_0/h$, p_0 is a constant expressing the value of the static magnetic potential. A normal harmonic mechanical excitation $\bar{\mathbf{F}}_t^T = \{0,0,0,0,0,0,0,0,1\}\sin(2\pi t)$ is applied on the top surface of plate.

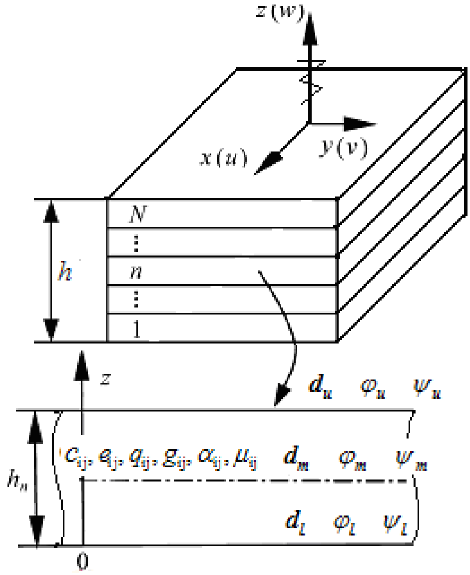

Figure 1: Mechanic model of FGM magneto-electro-elastic plate.

Eq. (32) can be written as:

$$\begin{aligned}
&-(2\pi)^2[M_s]_t\frac{\partial\{\Re\}_t}{\partial\theta}+[[K_{dd}]_t+[\Gamma]_t+[\Upsilon]]\frac{\partial\{\Re\}_t}{\partial\theta}+\frac{\partial[K_{dd}]_t}{\partial\theta}\{\Re\}_t=\{0\}\\
&[\Gamma]_t=[K_{d\varphi}]_t\left[[K_{\varphi\psi}]_t^{-1}[K_{\varphi\varphi}]_t-[K_{\psi\psi}]_t^{-1}[K_{\varphi\psi}]_t^{\mathrm{T}}\right]^{-1}\left[[K_{\varphi\psi}]_t^{-1}[K_{d\varphi}]_t^{\mathrm{T}}-[K_{\psi\psi}]_t^{-1}[K_{d\psi}]_t^{\mathrm{T}}\right]\\
&[\Upsilon]_t=[K_{d\psi}]_t\left[[K_{\varphi\psi}]_t^{-\mathrm{T}}[K_{\psi\psi}]_t-[K_{\varphi\varphi}]_t^{-1}[K_{\varphi\psi}]_t\right]^{-1}\left[[K_{\varphi\psi}]_t^{-\mathrm{T}}[K_{d\psi}]_t^{\mathrm{T}}-[K_{\varphi\varphi}]_t^{-1}[K_{d\varphi}]_t^{\mathrm{T}}\right]
\end{aligned} \tag{33}$$

$\frac{\partial\{\varphi\}_t}{\partial\theta}$ and $\frac{\partial\{\Psi\}_t}{\partial\theta}$ can be obtained from the last two equations of Eq. (32)

$$\begin{cases}
\frac{\partial\{\Phi\}_t}{\partial\theta}=\left\{\left[[K_{\varphi\psi}]_t^{-1}[K_{\varphi\varphi}]_t-[K_{\psi\psi}]_t^{-1}[K_{\varphi\psi}]_t^{\mathrm{T}}\right]^{-1}\left[[K_{\varphi\psi}]_t^{-1}[K_{d\varphi}]_t^{\mathrm{T}}-[K_{\psi\psi}]_t^{-1}[K_{d\psi}]_t^{\mathrm{T}}\right]\right\}\frac{\partial\{\Re\}_t}{\partial\theta}\\
\frac{\partial\{\Psi\}_t}{\partial\theta}=\left\{\left[[K_{\varphi\psi}]_t^{-\mathrm{T}}[K_{\psi\psi}]_t-[K_{\varphi\varphi}]_t^{-1}[K_{\varphi\psi}]_t\right]^{-1}\left[[K_{\varphi\psi}]_t^{-\mathrm{T}}[K_{d\psi}]_t^{\mathrm{T}}-[K_{\varphi\varphi}]_t^{-1}[K_{d\varphi}]_t^{\mathrm{T}}\right]\right\}\frac{\partial\{\Re\}_t}{\partial\theta}
\end{cases} \tag{34}$$

$\frac{\partial w}{\partial v}$ is defined as sensitivity of a variable 'w' to a parameter 'v'. $\frac{\partial w}{\partial v}$ has the physical meaning as shown below:

$$\Delta w=\frac{\partial w}{\partial v}\Delta v \tag{35}$$

$$\text{For} \quad \frac{\partial w}{\partial v} > 0 \quad \text{and} \quad \Delta v > 0, \ \Delta w > 0. \tag{36}$$

$$\text{For} \quad \frac{\partial w}{\partial v} < 0 \quad \text{and} \quad \Delta v > 0, \ \Delta w < 0 \tag{37}$$

We first obtain $\{\Re\}_t$ from the solution of Eq. (30), and then obtain $\frac{\partial\{\Re\}_t}{\partial\theta}$ by substituting $\{\Re\}_t$ into Eq. (33) and solving Eq. (33). The numerical results are obtained by MATLAB program, and the figures are plotted by Origin 8.

Fig. 2 shows the sensitivity distributions of the dimensionless deflection amplitude of the plate to elastic parameters $C^l\,(i,j)$ across the thickness for $\eta = 1$. It is observed from Fig. 2 that dimensionless deflection amplitudes of both the surfaces $\bar{z} = 0.1$ and $\bar{z} = 0.87$ is hardly sensitive to all the elastic parameters The dimensionless deflection amplitude is the most sensitive to the two parameters $C^l\,(1,2)$ and $C^l\,(2,2)$, however, $C^l\,(1,2)$ and $C^l\,(2,2)$ have opposite effects on vibration control. In other words, the parameter $C^l\,(2,2)$, when increase, can suppress the vibration, but $C^l\,(1,2)$ when increase, can cause the more strong vibration The dimensionless deflection amplitude is insensitive to elastic parameter $C^l\,(5,5)$. Sensitivities of the dimensionless deflection amplitudes between $\bar{z} = 0.1$ and $\bar{z} = 0.87$ to $C^l\,(1,2)$ and $C^l\,(1,3)$ are positive; to $C^l\,(1,1)\,C^l\,(2,2)$, $C^l\,(6,6)$ and $C^l\,(4,4)$ are negative. A positive sensitivity means that the amplitude increases with the increase of parameters, while a negative sensitivity instead.

Fig. 3 shows the sensitivity distributions of the dimensionless deflection amplitude of the plate to elastic parameters $C^l\,(i,j)$ across the thickness for $\eta = 3$ and $\eta = 10$, respectively. It is seen from Fig. 3 that deflection amplitude is the most sensitive to elastic parameter $C^l\,(6,6)$, the dimensionless deflection amplitudes of both the surfaces $\bar{z} = 0.85$ for $\eta = 3$ and $\bar{z} = 0.78$ for $\eta = 10$ are hardly sensitive to all the elastic parameters. In Fig, 2 it is medium, but in Fig. 3 the absolute value of sensitivity of the dimensionless deflection amplitude of the plate to $C^l\,(6,6)$ is the largest namely, the relative sensitivity of the dimensionless deflection amplitude of the plate to $C^l\,(6,6)$ will increase with the increase of exponent factor 'η'.

In Fig. 4 the first two digital in $Cijkl$ namely ij denotes $C^l\,(i,j)$, and the next k or kl denotes the value of η, such as $C1110$ denotes the elastic constant $C^l\,(1,1)$ and $\eta = 10$. It is seen from Fig. 4 that as the exponent factor 'η' increases the magnitude of sensitivity of the dimensionless deflection amplitude of the plate to the elastic parameters decreases.

Fig. 5 shows the sensitivity distributions of the dimensionless electric potential amplitudes of the plate to elastic parameter $C^l\,(i,j)$ across the thickness ($\eta = 1$). It is seen from the Fig. 5 that the dimensionless electric potential amplitudes of the plate are the most sensitive to the two elastic parameters $C^l\,(1,2)$ and $C^l\,(1,1)$. However,

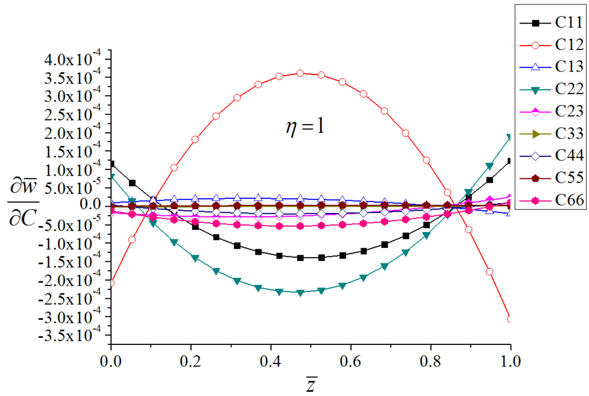

Figure 2: Sensitivity distributions of the dimensionless deflection amplitude of the plate to elastic parameters $C^l\,(i,j)$ across the thickness ($\eta = 1$).

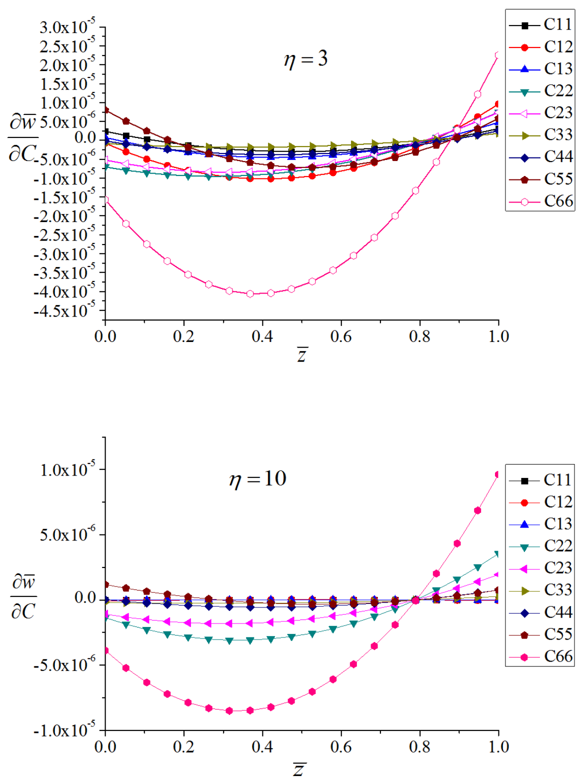

Figure 3: Sensitivity distributions of the dimensionless deflection amplitude of the plate to elastic parameters $C^l\,(i,j)$ across the thickness ($\eta = 3$ and $\eta = 10$).

$C^l(1,2)$ and $C^l(1,1)$ have opposite effects on vibration control namely, $C^l(1,1)$, when increase, can suppress the vibration of electric potential, but $C^l(1,2)$, when increase, can lead to the more strong vibration of electric potential The dimensionless electric potential amplitudes is hardly sensitive to these elastic parameters $C^l(3,3)$, $C^l(4,4)$ and $C^l(5,5)$. Sensitivity curves of the electric potential amplitude to these elastic parameters $C^l(1,1)$, $C^l(1,2)$ and $C^l(2,2)$ are parabola The dimensionless electric potential amplitude of the top surface of the plate is hardly sensitive to all the elastic parameters. Sensitivity of the dimensionless electric potential amplitude of the plate to the elastic parameters $C^l(1,2)$, $C^l(1,3)$ and $C^l(6,6)$ are positive; to the elastic parameters $C^l(1,1)$, $C^l(2,2)$ and $C^l(2,3)$ are negative.

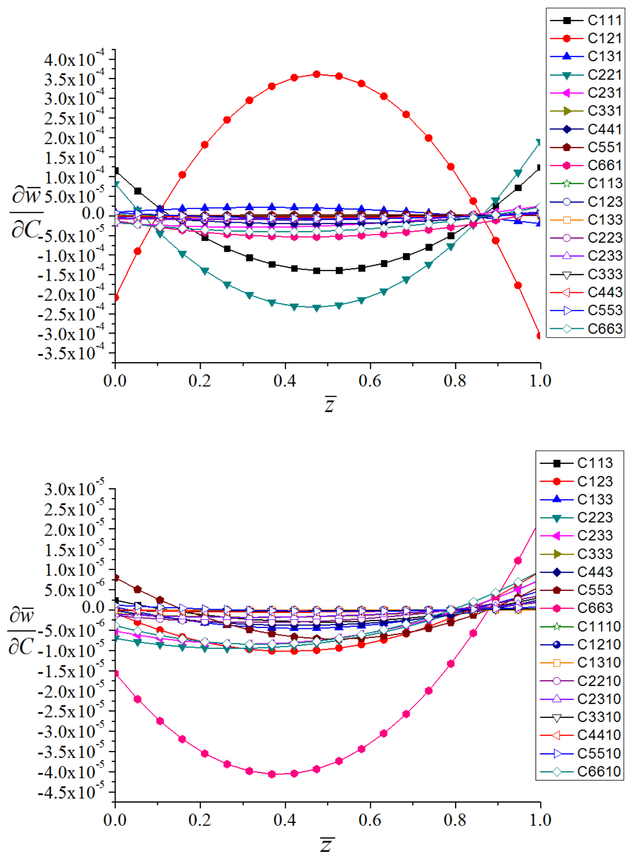

Figure 4: Sensitivity distributions of dimensionless deflection amplitude of the plate to elastic parameters $C^l(i,j)$ across the thickness ($\eta = 1\eta = 3$, $\eta = 10$).

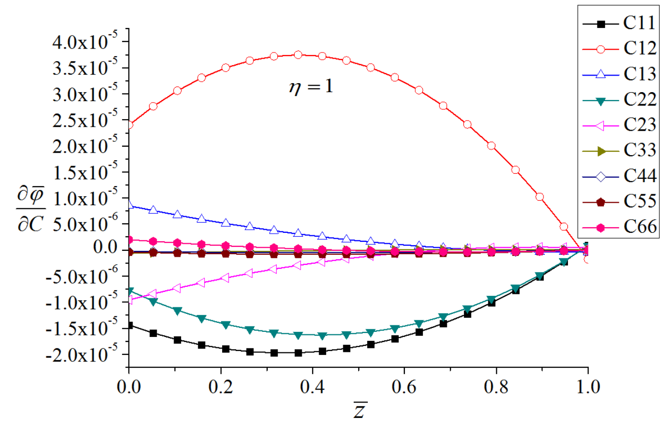

Figure 5: Sensitivity distributions of the dimensionless electric potential amplitudes of the plate to elastic parameter $C^l\,(i,j)$ across the thickness ($\eta = 1$).

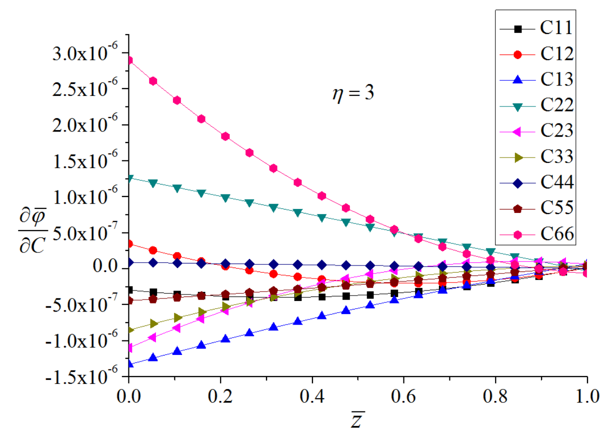

Figure 6: Sensitivity distributions of the dimensionless electric potential amplitudes of the plate to elastic parameter $C^l\,(i,j)$ across the thickness ($\eta = 3$).

The sensitivity distributions of the dimensionless electric potential amplitudes of the plate to elastic parameter $C^l\,(i,j)$ across the thickness ($\eta = 3$) is shown in Fig. 6. It can be seen from Fig. 6 that magnitude of sensitivity of the dimensionless electric potential amplitudes of the plate to elastic parameter $C^l\,(i,j)$ gradually reduce from the bottom surface ($\bar{z} = 0$) to the top surface of the plate ($\bar{z} = 1$) The dimensionless electric potential amplitudes of the plate is hardly sensitive to elastic parameter $C^l(4,4)$ regardless of $\eta = 1$ or $\eta = 3$. It has been noticed from Fig. 5 that for $\eta = 1$, $\frac{\partial \bar{\varphi}}{\partial C^l(1,3)} > 0$, $\frac{\partial \bar{\varphi}}{\partial C^l(1,2)} > 0$, $\frac{\partial \bar{\varphi}}{\partial C^l(2,2)} < 0$. Nevertheless, in Fig. 6 for $\eta = 3$, $\frac{\partial \bar{\varphi}}{\partial C^l(1,3)} < 0$, $\frac{\partial \bar{\varphi}}{\partial C^l(1,2)} < 0$, $\frac{\partial \bar{\varphi}}{\partial C^l(2,2)} > 0$. The physical meaning is that for $\eta = 1$, $C^l(1,2)$ and $C^l(1,3)$, when increase, can cause the more strong vibration of electric potential, and $C^l(2,2)$, when increase, can suppress vibration of electric potential, however, For $\eta = 3$, $C^l(1,2)$, $C^l(1,3)$ and $C^l(2,2)$ have the opposite effects on vibration as compared with for $\eta = 1$.

Fig. 7 shows the sensitivity distributions of the dimensionless electric potential amplitudes of the plate to elastic parameter $C^l(i,j)$ across the thickness for $\eta = 1$, $\eta = 3$, $\eta = 10$, respectively. It is also seen from the comparison of the sensitive curves for $\eta = 1$, $\eta = 3$ and $\eta = 10$ in Fig. 7 that as the exponent 'η' increases the magnitudes of sensitivity of the dimensionless electric potential amplitudes of the plate to the elastic parameters decrease.

Fig. 8 shows the sensitivity distribution of the dimensionless magnetic potential amplitude of the plate to the elastic parameter $C^l(i,j)$ across the thickness ($\eta = 1$). It has been noticed that sensitivity curves of the magnetic potential amplitude to these elastic parameters $C^l(1,1)$, $C^l(1,2)$, $C^l(1,3)$, $C^l(2,2)$, $C^l(2,3)$ are parabola. Further it is seen from Fig. 8 that the dimensionless magnetic potential amplitudes of the plate are the most sensitive to the two elastic parameters $C^l(1,2)$ and $C^l(1,1)$. However, $C^l(1,2)$ and $C^l(1,1)$ have opposite effects on vibration control. $C^l(1,1)$, when increase, can suppress vibration of magnetic potential, but $C^l(1,2)$, when increase, can cause the more strong vibration of magnetic potential The values of sensitivity of magnetic potential to these elastic parameters $C^l(1,2)$, $C^l(1,3)$, $C^l(2,3)$ and $C^l(6,6)$ are positive; to these elastic parameters $C^l(1,1)$ and $C^l(2,2)$ are negative. The dimensionless magnetic potential amplitude of the plate is hardly sensitive to $C^l(3,3)$, $C^l(4,4)$ and $C^l(5,5)$.

The sensitivity distributions of the dimensionless magnetic potential amplitudes of the plate to elastic parameter $C^l(i,j)$ across the thickness ($\eta = 3$) is shown in Fig. 9. It can be seen from Fig. 9 that magnitude of sensitivity to elastic parameter $C^l(i,j)$ gradually reduce from the bottom surface ($\bar{z} = 0$) to the top surface ($\bar{z} = 1$) of the plate. The dimensionless magnetic potential amplitude of the plate is hardly sensitive to the elastic parameter $C^l(4,4)$. In Fig.8 it is very small, but in Fig. 9 magnitude of sensitivity of magnetic potential amplitude to the elastic parameter $C^l(6,6)$ is larger than that to the other parameters except for $C^l(1,2)$. In other words, as the exponent factor 'η' increases the relative sensitivity of the dimensionless magnetic potential amplitude of the plate to the elastic parameter $C^l(6,6)$ increases.

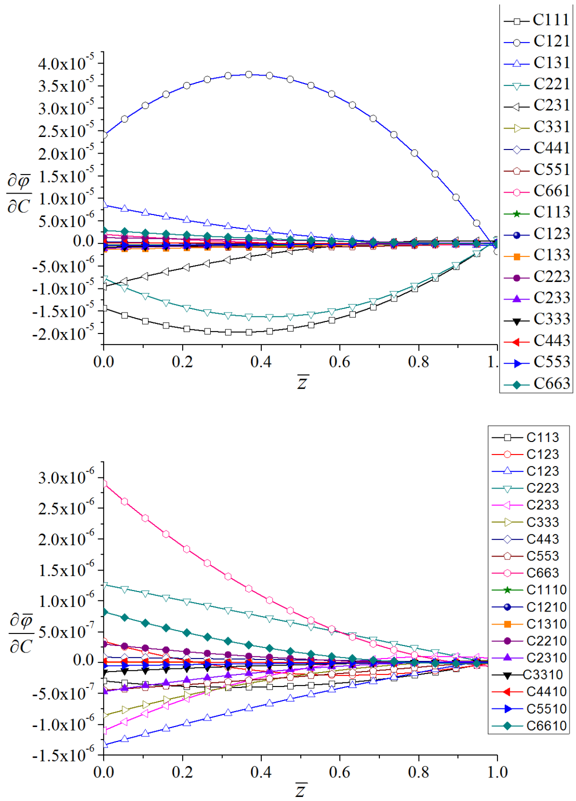

Figure 7: Sensitivity distributions of the dimensionless electric potential amplitudes of the plate to elastic parameter $C^l\,(i,j)$ across the thickness ($\eta = 1\eta = 3,,\eta = 10$).

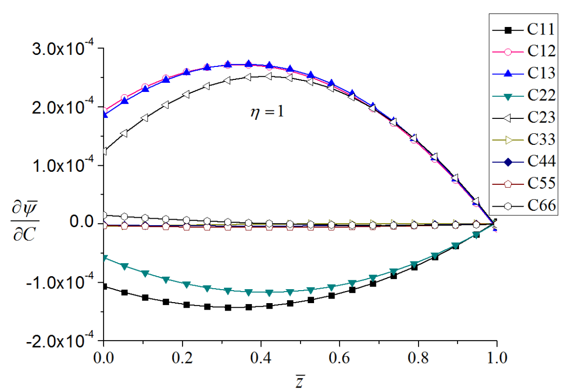

Figure 8: Sensitivity distribution of the dimensionless magnetic potential amplitude of the plate to the elastic parameter $C^l\,(i,j)$ across the thickness ($\eta = 1$).

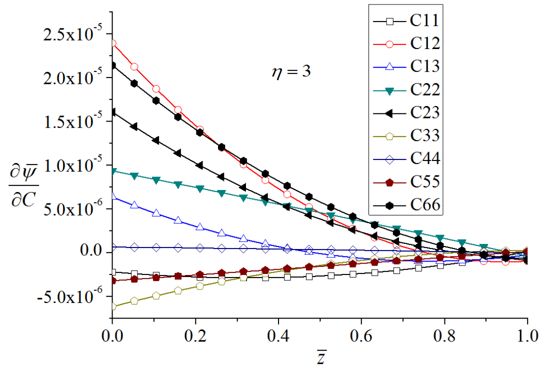

Figure 9: Sensitivity distribution of the dimensionless magnetic potential amplitude of the plate to the elastic parameter $C^l\,(i,j)$ across the thickness ($\eta = 3$).

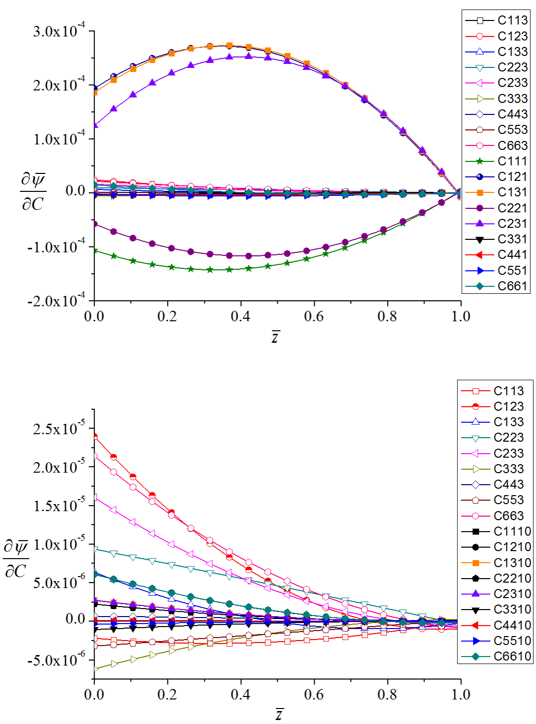

Figure 10: Sensitivity distribution of the dimensionless magnetic potential amplitude of the plate to the elastic parameter $C^l\,(i,j)$ across the thickness ($\eta = 1\eta = 3,,\eta = 10$).

Fig. 10 shows the sensitivity distribution of the dimensionless magnetic potential amplitude of the plate to the elastic parameter $C^l(i,j)$ across the thickness, for $\eta = 1\eta = 3$, $\eta = 10$, respectively. It is seen from the comparison of the sensitive curves for $\eta = 1$, $\eta = 3$, $\eta = 10$ that magnitude of sensitivity of the dimensionless magnetic potential amplitude of the plate to the elastic parameters decreases as the exponent factor 'η' increases.

5 Conclusion

We can obtain the following conclusions from the numerical example:

1. For $\eta = 1$ the sensitivity curves of the dimensionless amplitude of the electric and magnetic potentials of the plate to these elastic parameters $C^l(1,1)$, $C^l(1,2)$ and $C^l(2,2)$ are parabola. But for $\eta = 3$ the parabola disappears as the exponent factor 'η' increases magnitude of the sensitivity to elastic parameter $C^l(i,j)$ reduce from the bottom ($\bar{z} = 0$) to the top surface ($\bar{z} = 1$) of the plate.

2. There is a surface within the plate. Deflection amplitude of the surface is hardly sensitive to all the elastic parameters.

3. The dimensionless electric and magnetic potential amplitudes of the top surface of the plate is hardly sensitive for all the elastic parameters no matter how much the exponent factor 'η' is.

4. The dimensionless amplitudes of electric potential, magnetic potential and elastic deflection are all insensitive to the elastic parameter $C^l(4,4)$.

5. The relative sensitivities of the dimensionless deflection, electric and magnetic potentials amplitude of the plate to $C^l(6,6)$ increase as the exponent factor 'η' increases.

6. As the exponent factor 'η' increases the sensitivity of dynamic response of the FGM plate to its elastic parameters decreases.

Acknowledgement: This work is supported by Foundation of China under the Grant Number 11372109.

References

Akbarzadeh, A. H.; Chen, Z. T. (2011): Magnetoelectroelastic behavior of rotating cylinders resting on an elastic foundation under hygrothermal loading. *Smart Mater. Struct.*, vol. 20, no. 6, pp. 0964-1724

Bishay, P. L.; Sladek, J.; Sladek, V.; Atluri, S. N. (2012): Analysis of Functionally Graded Magneto-Electro-Elastic Composites Using Hybrid/Mixed Finite Elements and Node-Wise Material Properties. *CMC: Computers, Materials & Continua*, vol. 29, no. 3, pp. 213-262.

Buchanan, G. R. (2004): Layered verses multiphase magneto-electro-elastic composites. *Composites B* (*Engg*) vol. 35, no. 5, pp. 413–420.

Harshe, G.; Dougherty, J. P.; Newnham, R. E. (1993): Theoretical modeling of multilayered magneto- electric composites. *Int. J. Appl. Electromag. Mater.,* no. 4, pp. 145–159.

Li, Y.; Zhang, J. (2014): Free vibration analysis of magneto-electro-elastic plate resting on a Pasternak foundation. *Smart Mater. Struct*., vol. 23, no. 2, pp. 0964-1726.

Pan, E. (2001): Exact solution for simply supported and multilayered magneto-electro-elastic plates. *J. Appl. Mech., ASME,* vol. 68, pp. 608–618.

Pan, E.; Heyliger, P. R. (2002): Free vibrations of simply supported and multilayered magneto-electro -elastic plates. *J. Sound Vib.*, vol. 252, no. 3, pp. 429–442.

Rajesh, K. Bhangale; Ganesan, N. (2006): Static analysis of simply supported functionally graded and layered magneto-electro -elastic plates. *Int. J. Solids Struct.,* vol. 43 no. 10, pp. 3230–3253.

Sedighi, M. R.; Shakeri, M. (2009): A three-dimensional elasticity solution of functionally graded piezoelectric cylindrical panels. *Smart. Mater. Struct*., vol. 18, no. 5, pp. 0964-1726.

Saadatfar, M.; Aghaie-Khafri, M. (2014): Hygrotherm-magneto-electro-elastic analysis of a functionally graded magneto-electro-elastic hollow sphere resting on an elastic foundation. *Smart Mater. Struct*., vol. 23, no. 3, pp. 0964-1726.

Wang, J.; Chen, L.; Fang, S. (2003): State vector approach to analysis of multilayered magneto- electro-elastic plates. *Int. J. Solids Struct*., vol. 40, no. 7, pp. 1669–1680.

Wang, J.; Li, X. (2008): Analytical solutions for the magnetoelectric effect of multilayered magneto-electro-elastic media. *Smart Mater. Struct*., vol.17, no.4, pp. 0964-1726.

Appendix A

The magnetic and electric parameters are given by:

$$\mathbf{C}^l = \begin{bmatrix} 79.7 & 35.8 & 35.8 & 0 & 0 & 0 \\ 35.8 & 79.7 & 35.8 & 0 & 0 & 0 \\ 35.8 & 35.8 & 66.8 & 0 & 0 & 0 \\ 0 & 0 & 0 & 17.2 & 0 & 0 \\ 0 & 0 & 0 & 0 & 14.4 & 0 \\ 0 & 0 & 0 & 0 & 0 & 14.4 \end{bmatrix} \mathrm{GP}a, \quad \mathbf{C} = \mathbf{C}^l e^{\eta z}$$

$$\boldsymbol{\mu}^l = \begin{bmatrix} 5.4 & 0 & 0 \\ 0 & 5.4 & 0 \\ 0 & 0 & 5.4 \end{bmatrix} \times 10^{-6}\mathrm{Vs.(Am)}^{-1}, \quad \boldsymbol{\mu} = \boldsymbol{\mu}^l e^{\eta z},$$

$$\mathbf{g}^l = \begin{bmatrix} 3.8 & 0 & 0 \\ 0 & 3.8 & 0 \\ 0 & 0 & 3.8 \end{bmatrix} \times 10^{-10}\mathrm{As}\cdot(\mathrm{Vm})^{-1}, \quad \mathbf{g} = \mathbf{g}^l e^{\eta z},$$

$$\mathbf{e}^l = \begin{bmatrix} 0 & 0 & 0 & 0 & 0 & 10.5 \\ 0 & 0 & 0 & 0 & 10.5 & 0 \\ -5.9 & -5.9 & 15.2 & 0 & 0 & 0 \end{bmatrix} \mathrm{c/m}^2, \quad \mathbf{e} = \mathbf{e}^l e^{\eta z}$$

$$\mathbf{q}^u = \begin{bmatrix} 0 & 0 & 0 & 0 & 0 & 108.3 \\ 0 & 0 & 0 & 0 & 108.3 & 0 \\ -60.9 & -60.9 & 156.8 & 0 & 0 & 0 \end{bmatrix} \mathrm{Vs/m}^2,$$

$$\mathbf{q} = \mathbf{q}^l e^{\eta z}, \quad \rho^l = 7454\mathrm{kg/m}^2, \quad \rho = \rho^l e^{\eta z}, \quad \boldsymbol{\alpha} = [0]_{3\times 3}\,.$$

Where the superscripts 'l' denotes the lower layer, 'η' is the exponential factor governing the degree of the material gradient in the z-direction.